

RESEARCH

Open Access



Safinamide, an inhibitor of monoamine oxidase, modulates the magnitude, gating, and hysteresis of sodium ion current

Te-Yu Hung¹, Sheng-Nan Wu^{2,3,4*} and Chin-Wei Huang^{5*}

Abstract

Background Safinamide (SAF), an α -aminoamide derivative and a selective, reversible monoamine oxidase (MAO)-B inhibitor, has both dopaminergic and nondopaminergic (glutamatergic) properties. Several studies have explored the potential of SAF against various neurological disorders; however, to what extent SAF modulates the magnitude, gating, and voltage-dependent hysteresis [$H_{ys(V)}$] of ionic currents remains unknown.

Methods With the aid of patch-clamp technology, we investigated the effects of SAF on voltage-gated sodium ion (Na_v) channels in pituitary GH3 cells.

Results SAF concentration-dependently stimulated the transient (peak) and late (sustained) components of voltage-gated sodium ion current (I_{Na}) in pituitary GH₃ cells. The conductance–voltage relationship of transient I_{Na} [$I_{Na(T)}$] was shifted to more negative potentials with the SAF presence; however, the steady-state inactivation curve of $I_{Na(T)}$ was shifted in a rightward direction in its existence. SAF increased the decaying time constant of $I_{Na(T)}$ induced by a train of depolarizing stimuli. Notably, subsequent addition of ranolazine or mirogabalin reversed the SAF-induced increase in the decaying time constant. SAF also increased the magnitude of window I_{Na} induced by an ascending ramp voltage V_{ramp} . Furthermore, SAF enhanced the $H_{ys(V)}$ behavior of persistent I_{Na} induced by an upright isosceles-triangular V_{ramp} . Single-channel cell-attached recordings indicated SAF effectively increased the open-state probability of Na_v channels. Molecular docking revealed SAF interacts with both MAO and Na_v channels.

*Correspondence:

Sheng-Nan Wu
snwu@mail.ncku.edu.tw

Chin-Wei Huang
huangcw@mail.ncku.edu.tw

¹Department of Pediatrics, Chi-Mei Medical Center, Tainan, Taiwan

²Department of Physiology, National Cheng Kung University Medical College, Tainan, Taiwan

³Institute of Basic Medical Sciences, National Cheng Kung University Medical College, Tainan, Taiwan

⁴School of Medicine, National Sun Yat-sen University, Kaohsiung, Taiwan

⁵Department of Neurology, National Cheng Kung University Hospital, College of Medicine, National Cheng Kung University, Tainan, Taiwan



© The Author(s) 2024. **Open Access** This article is licensed under a Creative Commons Attribution 4.0 International License, which permits use, sharing, adaptation, distribution and reproduction in any medium or format, as long as you give appropriate credit to the original author(s) and the source, provide a link to the Creative Commons licence, and indicate if changes were made. The images or other third party material in this article are included in the article's Creative Commons licence, unless indicated otherwise in a credit line to the material. If material is not included in the article's Creative Commons licence and your intended use is not permitted by statutory regulation or exceeds the permitted use, you will need to obtain permission directly from the copyright holder. To view a copy of this licence, visit <http://creativecommons.org/licenses/by/4.0/>. The Creative Commons Public Domain Dedication waiver (<http://creativecommons.org/publicdomain/zero/1.0/>) applies to the data made available in this article, unless otherwise stated in a credit line to the data.

Conclusion SAF may interact directly with Na_v channels in pituitary neuroendocrine cells, modulating membrane excitability.

Keywords Safinamide, Monoamine oxidase B, Voltage-gated sodium current, Window sodium ion current, Persistent sodium ion current, Voltage-dependent hysteresis

Background

Safinamide [SAF; (S)-2-((4-((3-fluorobenzyl)oxy)benzyl)amino)propanamide], an α -aminoamide derivative, is an oral drug used as either an anticonvulsant or an add-on treatment for Parkinson's disease when a patient is having an "off" episode [1–18]. However, although this compound was formerly investigated as an anticonvulsant, it has not been approved as a standard antiseizure medication in humans. Several studies also reported the efficacy of SAF as an add-on treatment to subthalamic nucleus deep brain stimulation [19, 20]. SAF exerts its effects through various mechanisms, including inhibition of monoamine oxidase (MAO)-B activity [2, 13–15, 21–24].

Other mechanisms may be involved in SAF-mediated modification of the functional activities [21]. SAF has been demonstrated to protect M17 neuronal cells against amyloid- β -induced oxidative stress and senescence [25]. The evidence supports the notion that SAF might lock Na_v channels into the inactivated stage to suppress Na^+ current [21, 26–29]. It also elevates blood pressure; SAF-induced hypertension may be associated with the inhibition of MAO-B activity [15, 23].

Voltage-gated Na^+ (Na_v) channels, which constitute whole-cell voltage-gated Na^+ currents, are essential for the generation, initiation, and propagation of action potentials in electrically excitable membranes. Nine α subunits of Na_v channels ($\text{Na}_v1.1$ – $\text{Na}_v1.9$) have been discovered across excitable mammalian tissues, including the central and peripheral nervous systems, the endocrine system, skeletal muscle, and the heart [29–32]. Upon brief depolarization, Na_v channels undergo a rapid transition from a resting state to an open state and then rapidly return to the inactivated state of the channel. The cumulative inhibition of I_{Na} during a train of depolarizing stimuli was demonstrated to affect the electrical behavior of excitable cells [33–36]. The window I_{Na} [$I_{\text{Na(W)}}$] has been reported to be responsible for background Na^+ conductance and varying firing patterns of action potentials [37–41]. The Hys_(V) of persistent I_{Na} [$I_{\text{Na(P)}}$] induced by a triangular ramp voltage (V_{ramp}) contributes to the electrical behavior [42, 43]. However, the effects of SAF on the magnitude, gating, and Hys_(V) behavior of I_{Na} remain to be clarified.

In light of the aforementioned observations, in the present study, we investigated the effects of SAF on the magnitude, gating, frequency dependence, and Hys_(V)

behavior of I_{Na} —including transient I_{Na} ($I_{\text{Na(T)}}$), late I_{Na} ($I_{\text{Na(L)}}$), $I_{\text{Na(W)}}$, and $I_{\text{Na(P)}}$ —in electrically excitable cells.

Methods

Chemicals, drugs, reagents, and solutions

SAF [PNU-151774E, Xadago, Equfina, and Fce-26743; (S)-2-((4-((3-fluorobenzyl)oxy)benzyl)amino)propanamide, (2S)-2-[[4-[(3-fluorophenyl)methoxy]phenyl]methylamino]propanamide;methanesulfonic acid, $\text{C}_{17}\text{H}_{19}\text{FN}_2\text{O}_2$, <https://pubchem.ncbi.nlm.nih.gov/compound/Safinamide>], dopamine, serotonin, tetraethylammonium chloride (TEA), and tetrodotoxin (TTX) were purchased from Sigma-Aldrich (Genechain, Kaohsiung, Taiwan). Metofluthrin was obtained from Chung Tai Sing Chemical Industry (Hsinchu, Taiwan), and mirogabalin (MGB) was obtained from Cayman Chemical (Genechain, Kaohsiung, Taiwan). Ham's F-12 Nutrient Mix, horse serum, fetal calf serum, L-glutamine, and trypsin/ethylenediaminetetraacetic acid (EDTA) were purchased from HyClone (Thermo Fisher, Tainan, Taiwan). All chemicals and reagents were of analytical grade.

The composition of the external or bath solution [4-(2-hydroxyethyl)-1-piperazineethanesulfonic acid (HEPES)-buffered normal Tyrode's solution] was as follows: 136.5 mM NaCl, 1.8 mM CaCl_2 , 5.4 mM KCl, 0.53 mM MgCl_2 , 5.5 mM glucose, and 5.5 mM HEPES–NaOH (pH 7.4). To measure K^+ currents (data not shown), we filled a patch pipette with an internal solution comprising 140 mM KCl, 1 mM MgCl_2 , 3 mM adenosine 5'-triphosphate disodium salt, 0.1 mM guanosine 5'-triphosphate disodium salt, 0.1 mM ethylene glycol tetraacetic acid, and 5 mM HEPES–KOH buffer (pH 7.2). To record the whole-cell I_{Na} , the K^+ in the internal solution was substituted with Cs^+ , and the pH of the solution was adjusted to 7.2 by adding cesium hydroxide. In the single-channel experiments performed to record Na_v currents, the pipette was filled with a Na^+ -rich solution containing 136 mM NaCl, 0.53 mM MgCl_2 , 5.5 mM glucose, and 5.5 mM HEPES–NaOH (pH 7.2). The bath medium was a K^+ -rich solution comprising 130 mM KCl, 10 mM NaCl, 3 mM MgCl_2 , 6 mM glucose, and 10 mM HEPES–KOH (pH 7.4). The solutions and culture media were generally filtered on the day of use by using sterile Acrodisc Syringe Filters containing a 0.2- μm Supor Membrane (Bio-Check; New Taipei City, Taiwan).

Cell preparations

GH₃ pituitary tumor cells, acquired from the Bioresources Collection and Research Center (number: 60,015; Hsinchu, Taiwan), were maintained in Ham's F-12 media containing 15% (v/v) horse serum, 2.5% (v/v) fetal calf serum, and 2 mM L-glutamine. Cells were grown in a monolayer culture at 37 °C in a humidified environment of carbon dioxide/air (1:19) for 5 or 6 days to a confluence of 60–80%. Trypsinization [0.025% trypsin solution (HyClone) containing 0.01 sodium N, N-diethyldithiocarbamate and EDTA] was performed for subculturing. The culture medium was changed every 2 or 3 days; cells were dispersed and passaged every 7–14 days. Experiments were performed after the cells had grown to a confluence of 60–80% (usually 5 or 6 days). The GH₃ cell line has been a reliable model for studying the molecular biology, pharmacology, and biophysics of electrically excitable cells, including pituitary endocrine cells.

Electrophysiological measurements

Shortly before experiments, GH₃ was carefully suspended in normal Tyrode's solution at room temperature (20–25 °C). A few drops of the suspension containing cell clumps were immediately added to a custom-built chamber on the stage of an inverted Diaphot-200 microscope (Nikon, Tokyo, Japan). Pipettes were pulled from Kimax-51 soft-glass capillaries (#34500-99; Kimble, Vineland, NJ) by using a Narishige PP-830 Vertical Puller (Tokyo, Japan), and their tips were fire-polished using a microforge (MF-83, Narishige). During the measurements, an electrode with a tip resistance of 2–4 MΩ, which was tightly inserted into a holder, was maneuvered using a WR-98 micromanipulator (Narishige). Patch-clamp experiments were performed in the voltage-clamp mode with either cell-attached or whole-cell configuration (rupturing of the membrane patch after GΩ formation) by using a RK-400 Patch-Clamp Amplifier (Bio-Logic, Claix, France) connected to a laptop [36, 44]. Shortly before GΩ formation, potential correction was performed for a liquid junction potential, which developed at the electrode's tip because of the difference in the compositions of the internal and bath solutions.

Data collection and recordings

Amplified signals were monitored using an HM-507 oscilloscope (Hameg, East Meadow, NY); the signals were recorded, digitized, and stored online at ≥10 kHz on a laptop (Sony VAIO CS series; Kaohsiung, Taiwan) connected to an Axon Digidata 1440A Digitizer (Molecular Devices) for efficient analog-to-digital and digital-to-analog conversion. Series resistance, always in the range of 6–18 MΩ, was electronically compensated to 80–95%. Voltage-activated currents recorded during whole-cell experiments were stored without leakage

correction. The digitizer was operated using pCLAMP (version 10.6; Molecular Devices) on Windows 10 (Microsoft Corporation, Redmond, WA, USA). To ensure digitalization, some recordings were digitally acquired using the PowerLab 2/26 system (AD Instruments; Kuoyang, New Taipei City, Taiwan). During the measurement, the solutions were exchanged through a homemade gravity-driven type of bath perfusion.

Data analyses

To evaluate the concentration-dependent stimulatory effects of SAF on I_{Na(T)} and I_{Na(L)}, I_{Na} was induced using a 30-ms depolarizing pulse (–100 to –10 mV). The amplitude of the current in SAF-treated and untreated cells was measured at the beginning [I_{Na(T)}] and end [I_{Na(L)}] of the voltage pulse. The duration of the voltage-clamp protocol is 30 msec and the I_{Na} displaying rapid activation and inactivation can be measured at the beginning and end of depolarizing pulse from –100 to –10 mV. The I_{Na(T)} of cells treated with 300 μM SAF was defined as 100% and compared with the current values obtained for different SAF concentrations. The concentration at which SAF increased 50% of the current [I_{Na(T)} or I_{Na(L)}] amplitude (EC₅₀) was determined using a three-parameter logistic model (modified version of the sigmoidal Hill equation) with goodness-of-fit evaluation:

$$\begin{aligned} & \text{Percentage increase (\%)} \\ & = \{E_{\max} \times [\text{SAF}]^{n_H}\} / \{EC_{50}^{n_H} + [\text{SAF}]^{n_H}\} \end{aligned}$$

where EC₅₀ is the SAF concentration ([SAF]) required for a 50% increase, n_H is the Hill slope, and E_{max} is the SAF-mediated maximal stimulation of I_{Na(T)} or I_{Na(L)}.

The sigmoidal relationship between V_{ramp}-induced I_{Na(W)} and the upsloping V_{ramp} (nonlinear current–voltage relationship) was investigated and fitted with the Boltzmann function as follows:

$$I/I_{\max} = G / \left\{ 1 + \exp \left[-\frac{(V - V_h)qF}{RT} \right] \right\} \times (V - E_{\text{rev}})$$

where V is the membrane potential in millivolts, E_{rev} is the reversal potential of I_{Na}, G is the I_{Na} conductance in nanosiemens, I is the current, V_h is the voltage at which half-maximal activation or inactivation of the current occurs, q is the apparent gating charge, F is Faraday's constant, R is the universal gas constant, and T is the absolute temperature.

The free energy ΔG₀ for the gating of I_{Na(W)} was determined by assuming a two-state gating model [equilibrium between closed (resting) and open states] of the Na_v channel. The ΔG₀ for the activation of I_{Na(W)} at

0 mV could be calculated as follows: $q \times F \times V_{1/2}$ [45, 46]. The standard errors in ΔG_0 ($\sigma_{qV_{1/2}}$) could be calculated as follows:

$$\sigma_{qFV_{1/2}} = F \times \sqrt{V_{1/2}^2 \sigma_q^2 + q^2 \sigma_{V_{1/2}}^2}$$

where σ_q and $\sigma_{V_{1/2}}$ represent the standard error in q and $V_{1/2}$, respectively.

Recordings and analyses of single-channel NaV currents

Single-channel Na_v currents induced by depolarizing pulses ranging from -100 to -10 mV were measured and subsequently analyzed using pCLAMP 10.7. The opening events of the channels were generally evaluated through multi-Gaussian adjustments of the distribution of amplitude across channels. Functional independence between channels was determined by comparing the observed stationary probabilities with the values calculated based on the binomial law. For dwell-time analyses, only a single channel was used in the patch-clamp experiment.

Curve-fitting approximations and statistical analyses

Linear or nonlinear curve fitting to different data sets was implemented using the least-squares minimization method through various maneuvers, including the Excel-embedded Solver (Microsoft Corporation) and 64-bit OriginPro (OriginLab; Scientific Formosa, Kaohsiung, Taiwan). The averaged results (whole-cell or single-channel data) are presented in terms of the mean \pm standard error of the mean; the number of independent samples (n) indicates the number of cells used for experimental data collection. Between-group differences were analyzed using paired or unpaired Student's *t*-test. The differences between more than two groups were evaluated through multiple comparisons performed using analysis of variance (ANOVA)-1 or ANOVA-2 with or without repeated-measures analysis, which was followed by a post-hoc Fisher's least-significant difference test. Statistical significance was set at $P < 0.05$ (indicated using *, **, or + in the figures).

Results

Effects of SAF on I_{Na} magnitude

We investigated the effects of SAF on the magnitude of I_{Na} induced by rapid membrane depolarization. The cells were bathed in Ca²⁺-free Tyrode's solution containing 10 mM TEA and 0.5 mM CdCl₂. TEA and CdCl₂ were used to block K⁺ and Ca²⁺ currents, respectively. The recording pipettes were filled with a solution containing Cs⁺. As shown in Fig. 1, the tested cell was maintained at -80 mV. Subsequently, a hyperpolarizing step was applied, bringing the voltage down to -100 mV for a duration of 30 ms. This was followed by a brief depolarization step

to -10 mV for 30 ms was applied to evoke I_{Na} . The voltage was then returned to -50 mV for 30 ms to observe the tail current, and finally, the voltage was returned to the holding potential. Depolarizing the voltage from -100 to -10 mV over 30 ms (from a holding potential of -100 mV) robustly induced an inward current with the properties of being rapidly activated and inactivated. The rapid inward current induced by the short depolarizing pulse was identified as I_{Na} [36, 47–49] because it could be blocked by TTX (1 μ M) and stimulated by either tefluthrin (Tef; 10 μ M) or metofluthrin (10 μ M). TTX is a potent inhibitor of I_{Na} ; Tef and metofluthrin effectively stimulate I_{Na} [39, 50, 51]. The results are summarized in Fig. 2.

SAF exposure resulted in gradual increases in the magnitudes of $I_{Na(T)}$ and $I_{Na(L)}$ induced by abrupt membrane depolarization pulses (Fig. 1A). For example, 1 min after the addition of 10 and 30 μ M SAF, the amplitude of $I_{Na(T)}$ had increased from a control value of 512 ± 23 pA ($n = 8$) to 1387 ± 131 pA ($n = 8$, $P < 0.05$) and 1991 ± 153 pA ($n = 8$, $P < 0.05$), respectively; the corresponding values for $I_{Na(L)}$ had increased from 18 ± 3 pA ($n = 8$) to 54 ± 9 pA ($n = 8$, $P < 0.05$) and 106 ± 17 pA ($n = 8$, $P < 0.05$), respectively. The amplitude of $I_{Na(L)}$ was measured at the end of the depolarizing pulse from -100 to -10 mV for a duration of 30 ms. After the removal of SAF, the amplitudes of $I_{Na(T)}$ and $I_{Na(L)}$ returned to 523 ± 24 and 20 ± 3 pA, respectively ($n = 8$). SAF (30 μ M) also increased the time constant $\tau_{inact(S)}$ corresponding to the slow component of $I_{Na(T)}$ inactivation, with no evident change in that corresponding to the fast component. As summarized in Fig. 3, SAF (30 μ M) markedly increased the $\tau_{inact(S)}$ of $I_{Na(T)}$ inactivation from 5.1 ± 0.7 to 10.2 ± 1.1 ms ($n = 8$, $P < 0.05$). Fig. 1B illustrates the time course of stimulatory effect of SAF (10 and 30 μ M) on I_{Na} . The presence of TTX (1 μ M) alone decreased $I_{Na(T)}$ and $I_{Na(L)}$ to 18 ± 2 pA ($n = 8$, $P < 0.05$) and 2 ± 1 pA ($n = 8$, $P < 0.05$), respectively, from a control value of 511 ± 17 pA and 32 ± 5 pA ($n = 8$).

SAF increased the amplitudes of $I_{Na(T)}$ and $I_{Na(L)}$ in a concentration-dependent manner (Fig. 1C). Using the Hill equation described in Materials and Methods, the EC₅₀ values corresponding to SAF-mediated stimulation of $I_{Na(T)}$ and $I_{Na(L)}$ were estimated to be 27.1 ± 2.1 and 4.8 ± 0.7 μ M, respectively. $I_{Na(T)}$ and $I_{Na(L)}$ induced by rapid depolarization pulses differentially increased in a concentration-dependent manner in GH₃ cells.

Effects of SAF on the steady-state I–V relationship and inactivation curve of $I_{Na(T)}$

To further characterize the stimulatory effects of SAF on $I_{Na(T)}$, we investigated whether this drug perturbs the steady-state I–V relationship of $I_{Na(T)}$ in GH₃ cells.

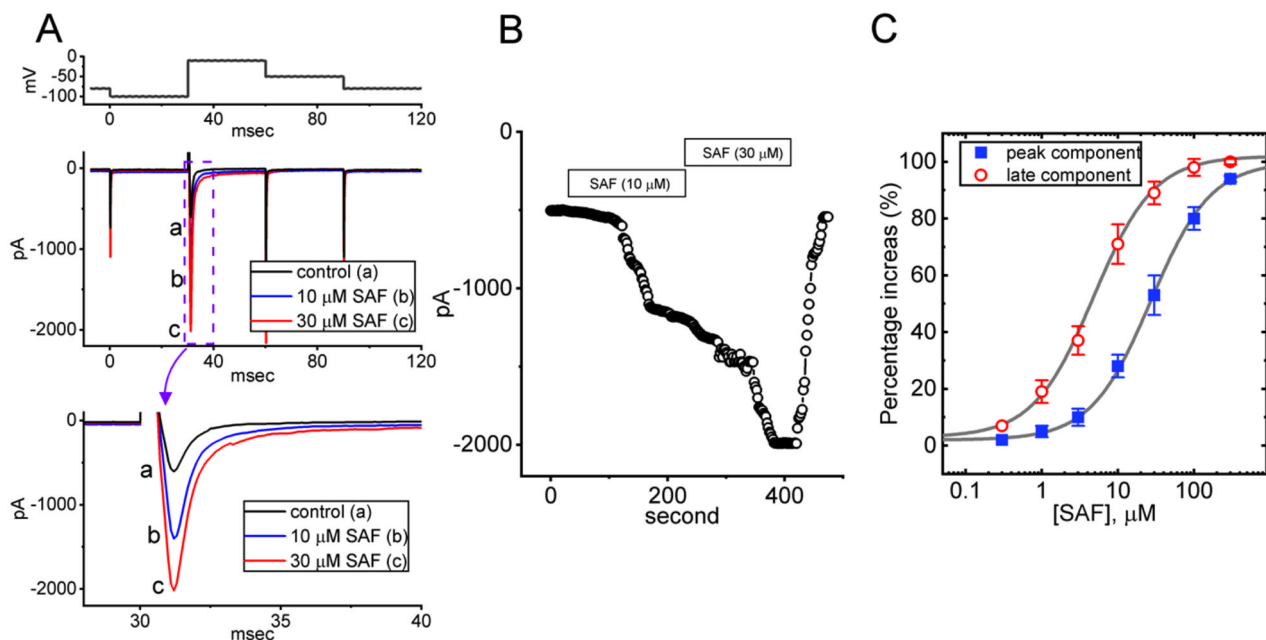


Fig. 1 Effect of safinamide (SAF) on the voltage-gated Na^+ current (I_{Na}) in pituitary tumor (GH₃) cells. To record macroscopic currents, calcium ion-free Tyrode's solution containing 10 mM tetraethylammonium chloride and 0.5 mM cadmium chloride was added to the cells; the recording electrode was filled with solution containing cesium ions. **(A)** Current traces during the control period (a, black; untreated cells) and during exposure to 10 (b, blue) and 30 (c, red) μM SAF. The voltage-clamp protocol used is indicated atop the current traces. In panel **A**, the third graph from the top is an expanded version of the second graph (purple dashed box). **(B)** Time course showing effect of 10 and 30 μM SAF on the amplitude of peak I_{Na} . Each current amplitude (indicated with black circles) was measured at the beginning of depolarizing pulse at a rate of 2 Hz. Horizontal bar shown above indicates the SAF application. **(C)** Concentration-response curves corresponding to SAF-mediated stimulation of transient I_{Na} [$I_{\text{Na(T)}}$; blue filled squares] and late I_{Na} [$I_{\text{Na(L)}}$; sustained; red open circles] in GH₃ cells (mean \pm standard error of the mean; $n = 8$ for each point). The gray smooth line indicates the goodness of fit of our model to the modified Hill equation. The EC_{50} values corresponding to the SAF-induced stimulation of $I_{\text{Na(T)}}$ and $I_{\text{Na(L)}}$ were 27.1 and 4.8 μM , respectively (least-squares minimization)

Fig. 4a illustrates $I_{\text{Na(T)}}$ traces induced by different voltage steps in the presence and absence of SAF. Fig. 4b depicts the mean I - V relationship of $I_{\text{Na(T)}}$ (i.e., V -shaped) in the absence and presence of 3 or 10 μM SAF. Fig. 4c also illustrates mean conductance versus voltage (G - V) relationship of $I_{\text{Na(T)}}$ obtained in the control period and with the addition of 3 or 10 μM SAF. The value required for half-maximal activation voltage was found to be shifted to more negative potentials in the presence of SAF. Additionally, the steady-state inactivation curve of I_{Na} was further characterized (Fig. 4d). In these experiments, a two-step voltage-clamp protocol was applied (indicated in the legend of Fig. 4d). The results showed that cell exposure to 10 μM SAF not only increased the maximal conductance of I_{Na} , but also shifted the inactivation curve to the rightward direction by approximately 14 mV with no change in the sloping factor of the curve.

Effects of dopamine, serotonin, SAF, SAF plus dopamine, and SAF plus serotonin on $I_{\text{Na(T)}}$ amplitude

Studies have demonstrated the existence of MAO activity in pituitary cells [52, 53]. In the inhibition of

MAO-B, the stimulatory effects of SAF on I_{Na} may result primarily from an increase in the extracellular concentration of dopamine or serotonin. We investigated whether dopamine or serotonin affects $I_{\text{Na(T)}}$ in these cells and whether the addition of dopamine and serotonin during SAF exposure reverses the SAF-mediated increase in I_{Na} . As shown in Fig. 5, the addition of neither dopamine nor serotonin altered the magnitude of $I_{\text{Na(T)}}$; similarly, during SAF exposure, the addition of neither dopamine nor serotonin reversed the SAF-mediated increase in $I_{\text{Na(T)}}$. Thus, under the experimental conditions employed in the present study, the SAF-mediated stimulation of $I_{\text{Na(T)}}$ in pituitary cells may not have involved the inhibition of MAO-B activity.

SAF-induced increase in the cumulative inhibition of $I_{\text{Na(T)}}$ during a train of depolarizing stimuli

The inactivation of $I_{\text{Na(T)}}$ has been demonstrated to accumulate before being elicited during repetitive short pulses [33, 34, 54]. SAF is efficacious as an add-on therapy following subthalamic nucleus deep brain stimulation in patients with Parkinson's disease [19, 20]. Therefore, we

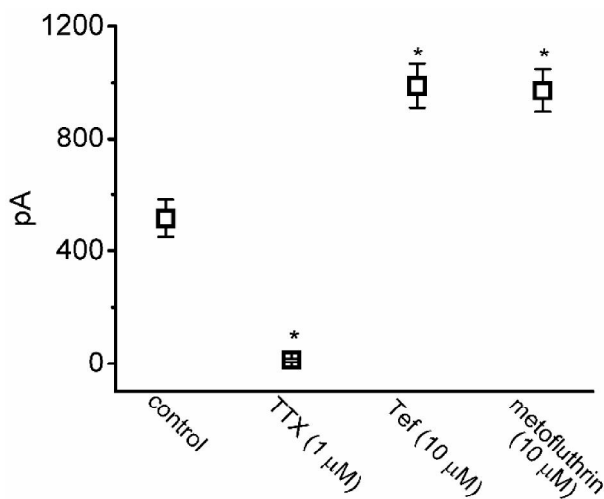


Fig. 2 Graph showing effects of tetrodotoxin (TTX), tefluthrin (Tef) and metofluthrin on the peak amplitude of I_{Na} in GH₃ cells. Current amplitude was measured at the beginning of each depolarizing pulse from -100 to -10 mV for a duration of 30 ms. Each point represents the mean \pm standard error of the mean ($n = 7$). The statistical analyses were done by ANOVA-1, $P < 0.05$, followed by *post-hoc* Fisher's least-significant different test, $P < 0.05$. *Significantly different from control ($P < 0.05$)

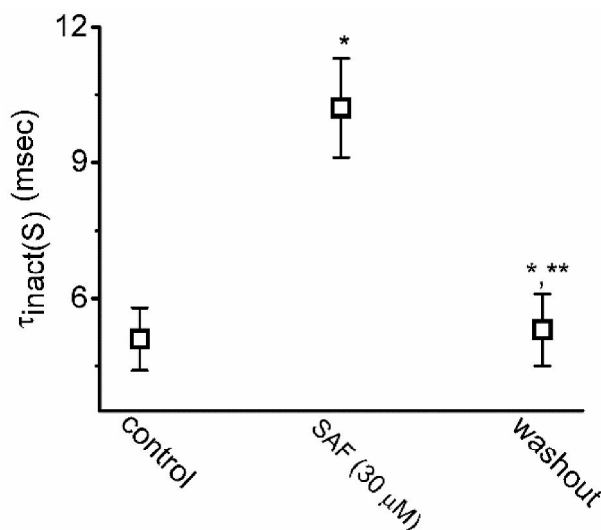


Fig. 3 Graph showing effects of SAF on the slow component ($\tau_{inact(S)}$) in inactivation time constant of I_{Na} in GH₃ cells. Each point represents the mean \pm standard error of the mean ($n = 8$). The statistical analyses were done by ANOVA-1, $P < 0.05$, followed by *post-hoc* Fisher's least-significant different test, $P < 0.05$. *Significantly different from control ($P < 0.05$) and **significantly different from SAF (30 μ M) alone group ($P < 0.05$)

investigated whether SAF could modify the inactivation of currents induced by a train of depolarizing stimuli. The test cells were maintained at -80 mV and subjected to repetitive depolarization to -10 mV (40 ms per pulse; rate

of 20 Hz; duration of 1 s). Similar to the findings of relevant studies [34, 36], during the control period (the absence of SAF), $I_{Na(T)}$ inactivation was noticed to be induced by 1 s of repetitive depolarization stimuli (-80 to -10 mV) with a decaying time constant of 65 ± 4 ms ($n = 7$; Fig. 6A, 6B and 6C). This indicated that the single-exponent process resulted in a sudden decay in the current. In the presence of 3 and 10 μ M SAF, the exponential time course of $I_{Na(T)}$ induced by the same train of depolarizing pulses was longer at 107 ± 5 ms ($n = 7$, $P < 0.05$) and 124 ± 6 ms ($n = 7$, $P < 0.05$), respectively. Furthermore, as MGB and ranolazine have been reported to suppress the amplitude of I_{Na} effectively [36, 47, 55, 56], we added ranolazine (Ran; 10 μ M) and mirogabalin (MGB; 10 μ M) separately in the presence of 10 μ M SAF. We found they effectively attenuated the SAF-induced increase in the decaying time constant of $I_{Na(T)}$ induced by a rapid train of pulses (Fig. 6B). The application of Ran (10 μ M) or MGB (10 μ M) alone decreased the decaying time constant of $I_{Na(T)}$ during the same train of depolarizing pulses to 39 ± 4 ms ($n = 7$, $P < 0.05$) or 42 ± 4 ms ($n = 7$, $P < 0.05$), respectively, from a control value of 66 ± 5 ms ($n = 7$). Thus, in addition to increasing the magnitude of $I_{Na(T)}$, SAF prominently affects the decaying of $I_{Na(T)}$ subjected to a 1-s train of depolarizing pulses.

Stimulatory effects of SAF on $I_{Na(W)}$

The induction of instantaneous $I_{Na(W)}$ by ascending (or upsloping) V_{ramp} has been demonstrated in various excitable cells [35, 36, 38, 40, 41, 48]. In the present study, we investigated whether the addition of SAF to GH₃ cells modulates the magnitude of $I_{Na(W)}$ induced by ascending V_{ramp} . Test cells were maintained at -80 mV and subjected to V_{ramp} ascending from -100 to $+40$ mV over 200 ms (i.e., ramp speed of 0.7 mV/ms) to induce $I_{Na(W)}$ [40, 48]. The amplitude and strength (Δ area) of $I_{Na(W)}$ induced by the ascending V_{ramp} sharply increased within 1 min of SAF exposure (Fig. 7A and 7B). The Δ area values of $I_{Na(W)}$ in the absence and presence of SAF and SAF plus Ran were calculated (Fig. 7B).

Effect of SAF on the activation energy required for the induction of $I_{Na(W)}$ by V_{ramp}

Experimental data points corresponding to $I_{Na(W)}$ were optimally fitted with the Boltzmann isotherm to estimate the values of q and $V_{1/2}$ for the instantaneous $I_{Na(W)}$ induced by V_{ramp} . Using these values, the ΔG_0 for the gating of $I_{Na(W)}$ activation at 0 mV in the absence and presence of SAF was calculated ($\Delta G_0 = q \times F \times V_{1/2}$; Fig. 7C). As the SAF concentration was increased, ΔG_0 for the induction of $I_{Na(W)}$ by a 200-ms-long V_{ramp} also increased; the subsequent addition of Ran effectively attenuated the SAF-mediated increase in ΔG_0 . In GH₃ cells exposed to 3 and 10 μ M SAF, the ΔG_0 values increased

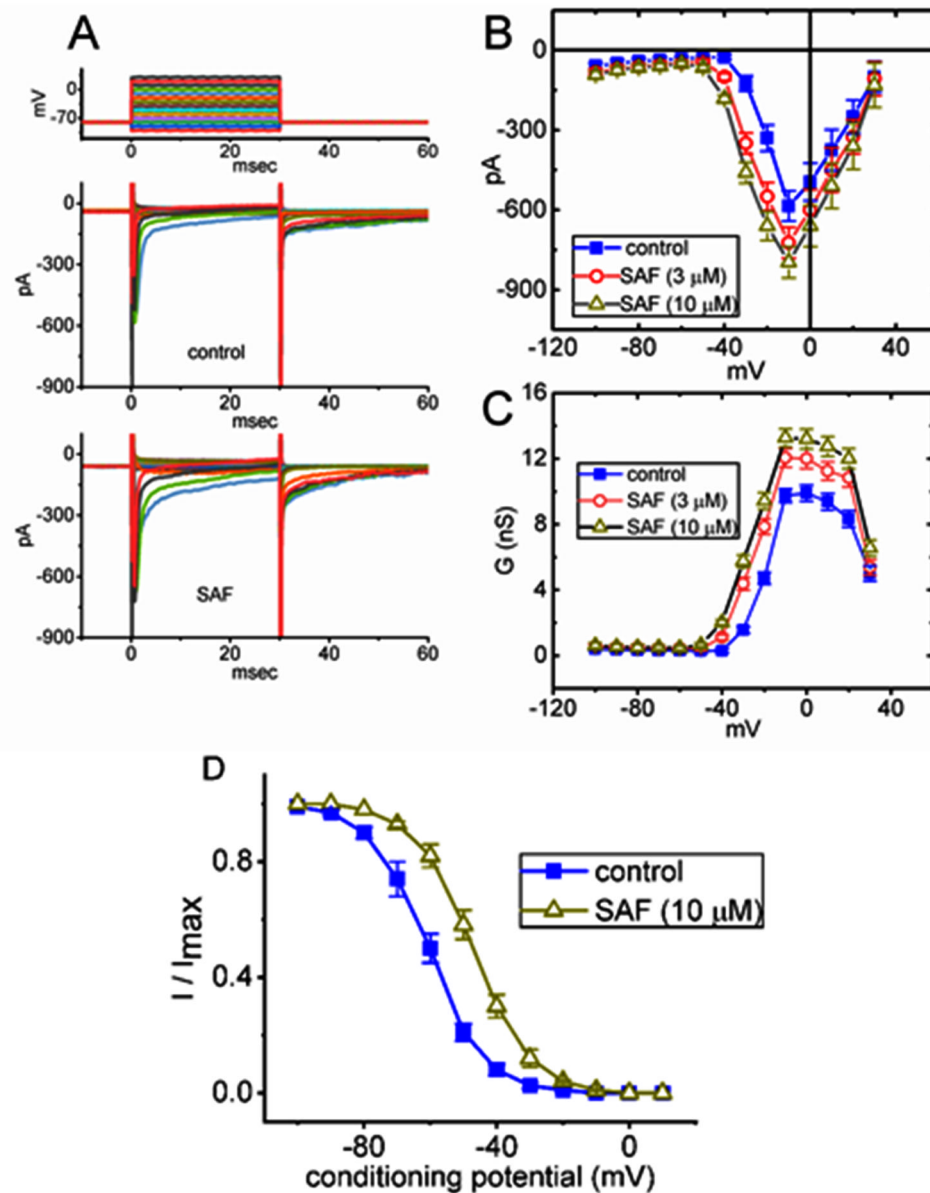


Fig. 4 Mean current–voltage (I - V) or conductance–voltage relationship of $I_{Na(T)}$ in GH₃ cells. The measurements were performed as described in the legend of Fig. 1. Because we used the whole-cell mode, the test cells were maintained at -80 mV and subjected to a series of command voltages ranging from -100 to $+30$ mV in 10 -mV increments. **(A)** Current traces during the control period (upper) and during the exposure to 3 μ M SAF. The voltage-clamp protocol used is indicated atop the current traces. **(B)** Mean I - V relationship of $I_{Na(T)}$ in the absence (blue filled squares) and with cell exposure to 3 μ M SAF (red open circles) or 10 μ M SAF (brown open triangles) (mean \pm standard error of the mean; $n = 8$ for each point). $I_{Na(T)}$ amplitude was measured at the beginning of each voltage pulse. Notably, the I - V relationship of $I_{Na(T)}$ (or peak I_{Na}) induced by 30 -ms voltage pulses was shifted to more negative potentials upon SAF (3 or 10 μ M) exposure. **(C)** Mean conductance versus voltage (G - V) of $I_{Na(T)}$ in the absence (blue filled squares) and with cell exposure to 3 μ M SAF (red open circles) or 10 μ M (brown open triangles) (mean \pm standard error of the mean; $n = 8$ for each point). The conductance–voltage relationship of $I_{Na(T)}$ was shifted to more negative potentials during exposure to SAF. **(D)** Effect of SAF (10 μ M) on the steady-state inactivation curve of $I_{Na(T)}$ (mean \pm standard error of the mean; $n = 7$ for each point). In these experiments, the conditioning voltage pulse with a duration of 30 ms to various membrane potentials between -100 and $+10$ mV was applied from a holding potential of -80 mV. Following each conditioning potential, a test pulse to -10 mV for a duration of 30 ms was given to activate I_{Na} . The normalized amplitude of I_{Na} (I/I_{max}) was constructed against the conditioning potential

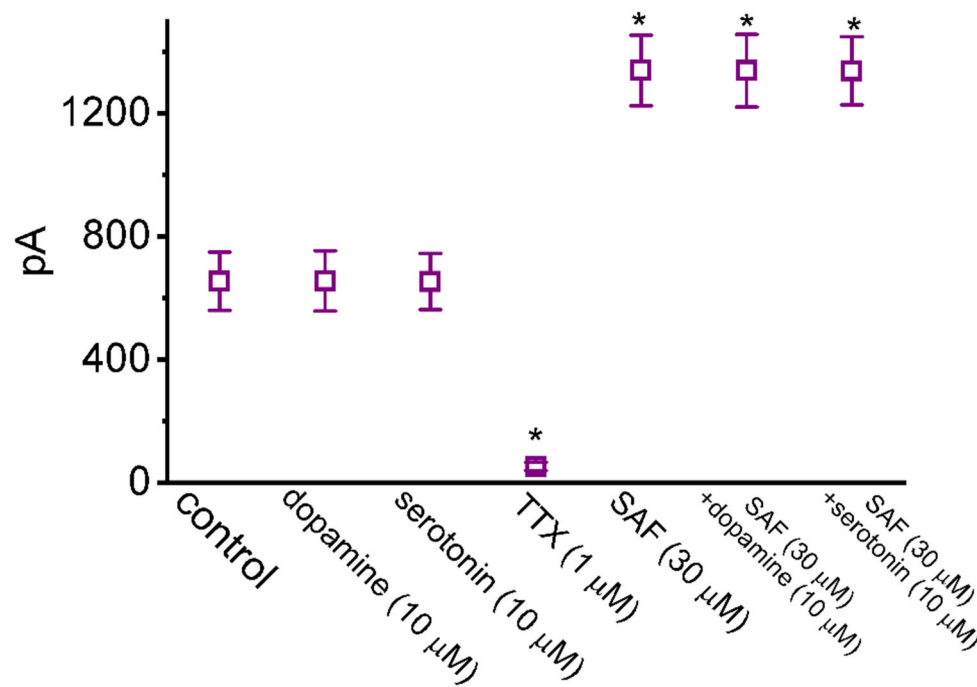


Fig. 5 Graph illustrating the effects of dopamine, serotonin, tetrodotoxin, SAF, SAF plus dopamine, and SAF plus serotonin on the amplitude of $I_{Na(P)}$ in GH₃ cells. Each current amplitude was measured at the beginning of a short depolarizing pulse (−100 to −10 mV). In the experiments of SAF plus dopamine and SAF plus serotonin, dopamine (10 μM) or serotonin (10 μM) was added when the cells were exposed to SAF (30 μM). Each point represents the mean ± standard error of the mean (n = 7). The statistical analyses were done by ANOVA-1, $P < 0.05$, followed by *post-hoc* Fisher's least-significant different test, $P < 0.05$. *Significantly different from control ($P < 0.05$)

from a control value of 6.78 ± 1.1 to 8.81 ± 1.6 kJ/mol (n = 7, $P < 0.05$) and 10.36 ± 1.8 kJ/mol (n = 7, $P < 0.05$), respectively.

Attenuation of the SAF-induced increase in the amplitude and $Hys_{(V)}$ of $I_{Na(P)}$ by MGB and Ran

We further investigated whether SAF exposure modulated the magnitude and $Hys_{(V)}$ behavior of $I_{Na(P)}$ induced by an isosceles-triangular V_{ramp} in GH₃ cells. To record whole-cell currents, the test cells were maintained at −80 mV and subjected to an upright isosceles-triangular V_{ramp} ascending from −110 and +50 mV over 3.2 s (digital-to-analog conversion; Fig. 8A). Consistent with the findings of relevant studies [43, 49, 57], we found that SAF exposure markedly increased the high and low amplitudes of $I_{Na(P)}$ induced by the upsloping (ascending) and downsloping (descending) ends of the upright triangular V_{ramp} , respectively; consequently, we observed a figure-of-eight (∞-shaped) configuration of the instantaneous I–V relationship for $I_{Na(P)}$ and found that the configuration was enhanced by SAF. For example, when test cells were subjected to an isosceles-triangular V_{ramp} over 3.2 s (ramp speed of 0.1 mV/ms), the $I_{Na(P)}$ amplitudes measured at −10 mV (high threshold) and −80 mV (low threshold) during the control period were 175 ± 14

pA (n = 7) and 288 ± 25 pA (n = 7), respectively. After the addition of 3 and 10 μM SAF, the $I_{Na(P)}$ amplitude at −10 mV [high-threshold $Hys_{(V)}$ loop] was 194 ± 17 pA (n = 7, $P < 0.05$) and 219 ± 18 pA (n = 7, $P < 0.05$), respectively; the corresponding amplitudes at −80 mV [low-threshold $Hys_{(V)}$ loop] were 348 ± 29 pA (n = 7, $P < 0.05$) and 389 ± 31 pA (n = 7, $P < 0.05$), respectively. Adding MGB and Ran separately during SAF exposure reversed the SAF-mediated increase in the high- and low-threshold $I_{Na(P)}$ induced by the triangular V_{ramp} (Fig. 8B). These findings indicate the unique $Hys_{(V)}$ behavior of $I_{Na(P)}$ induced by an isosceles-triangular V_{ramp} in GH₃ cells; SAF exposure may increase the strength of $Hys_{(V)}$.

Effect of SAF on single-channel Na_V currents

To elucidate the mechanisms underlying the effects of SAF on the magnitude of I_{Na} , we investigated the actions of SAF and SAF plus MGB on single-channel Na_V currents. This experiment was performed using the cell-attached configuration of the voltage-clamp test. Test cells were placed in K^+ -rich solution, and the recording pipette was filled with Na^+ -rich solution. SAF (10 μM) increased channel activity and decelerated current inactivation when the cells were exposed to depolarization stimuli ascending from −100 to −10 mV (rate of 0.1 Hz;

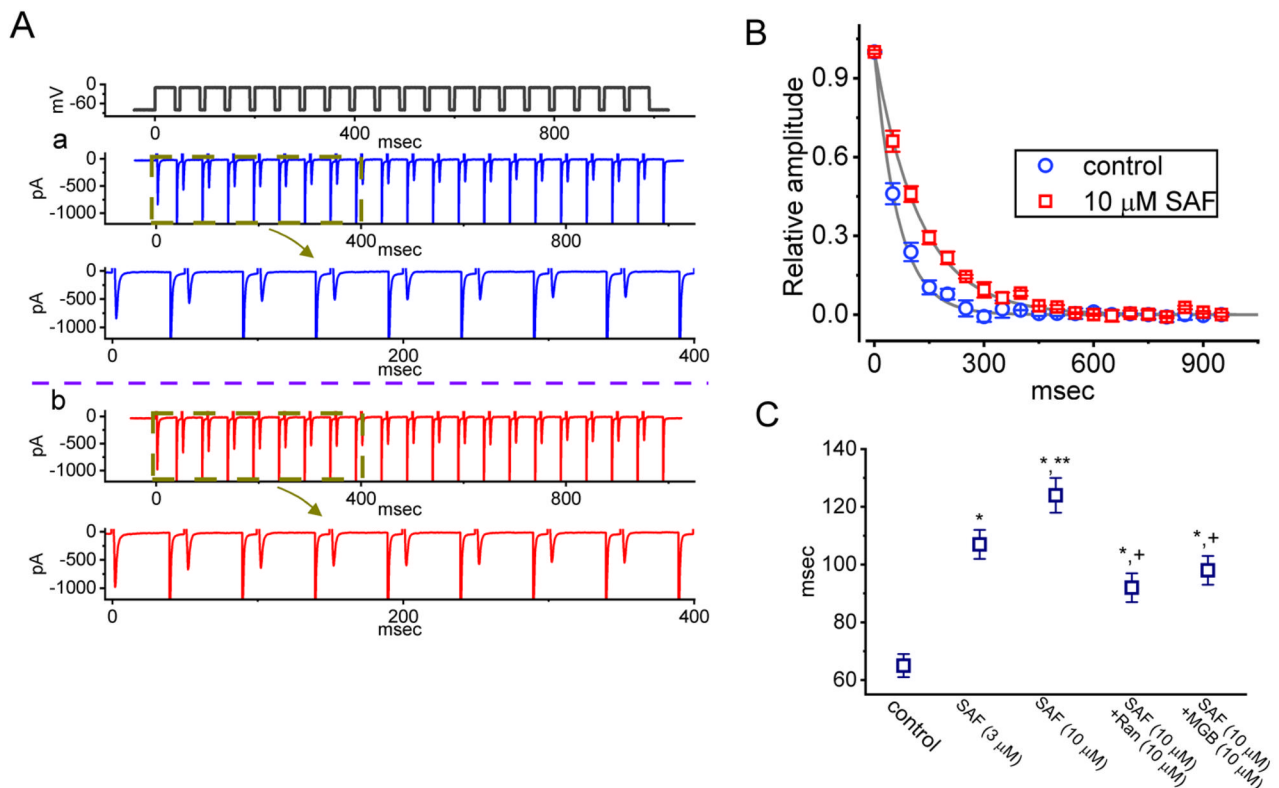


Fig. 6 Effect of SAF on $I_{Na(T)}$ decay induced by a train of depolarizing pulses in GH₃ cells. The train of pulses comprised twenty 40-ms pulses (voltage increased to -10 mV) with 10-ms intervals at -80 mV for a total duration of 1 s. **(A)** Current traces during the control period (a, blue) and during exposure to $10 \mu\text{M}$ SAF (b, red). The voltage-clamp protocol used is indicated atop the current traces. In panel **A**, the third graphs (blue and red) from the top are the expanded forms of the second graphs (brown dashed boxes). **(B)** The relative amplitude of $I_{Na(T)}$ versus pulse train duration in the absence (blue open circles) and presence (red open squares) of $10 \mu\text{M}$ SAF (mean \pm standard error of the mean; $n = 7$ for each point). The $I_{Na(T)}$ amplitudes were normalized by dividing the current amplitudes at the end of each pulse-train stimulation by those obtained at the beginning of the pulse train stimulation. The gray continuous lines on which the data points are overlaid are reliably fitted with a single exponential. **(C)** Summary graph depicting the effects of SAF (3 and $10 \mu\text{M}$), SAF plus ranolazine (Ran), and SAF plus MGB on the decaying time constant of the current induced by a train of depolarizing command voltages ranging from -80 to -10 mV (mean \pm standard error of the mean; $n = 7$ for each point). *Significantly different from the control ($P < 0.05$), **significantly different from the SAF ($3 \mu\text{M}$) alone group ($P < 0.05$), and +significantly different from the SAF ($10 \mu\text{M}$) alone group ($P < 0.05$)

Fig. 9A). Furthermore, the addition of MGB ($10 \mu\text{M}$) in the presence of $10 \mu\text{M}$ SAF reduced the probability of channel opening. The addition of $10 \mu\text{M}$ SAF markedly increased channel activity from 0.027 ± 0.007 to 0.091 ± 0.006 ($n = 7$, $P < 0.05$); the addition of $10 \mu\text{M}$ MGB in the presence of SAF reduced the open-state probability of the channel to 0.041 ± 0.007 ($n = 7$, $P < 0.05$). Moreover, with the presence of $10 \mu\text{M}$ SAF, the mean open time of Na_v channels was prolonged to 6.5 ± 0.7 ($n = 7$, $P < 0.05$) msec from a control value of 2.3 ± 0.3 msec ($n = 7$). However, no considerable modifications were noted in the amplitude of the single-channel current in the presence of SAF or SAF plus MGB (control, 2.01 ± 0.35 pA; SAF, 2.03 ± 0.37 pA; SAF plus MGB, 2.00 ± 0.44 pA; $n = 7$; $P > 0.05$). Consistent with these findings, the mean open time of the Na_v channel in the presence of $10 \mu\text{M}$ SAF (5.9 ± 1.1 ms; $n = 7$; $P < 0.05$)

was longer than that in the control period (2.3 ± 0.3 ms, $n = 7$); the subsequent further addition of $10 \mu\text{M}$ MGB decreased the mean open time to 3.7 ± 0.7 ms ($n = 7$, $P < 0.05$) (Fig. 9B). Although SAF did not change the amplitude of single-channel currents, it enhanced channel activity and decelerated inactivation of Na_v-channel opening in GH₃ cells. MGB added during SAF exposure reversed the SAF-induced increase in Na_v channel activity.

Docking prediction of SAF on human MAO_B and Na_v channel

Using PyRx, we further explored the molecular docking between human MAO-B (structure: <https://www.rcsb.org/structure/1GOS>) and SAF. Figure 10 illustrates the predicted binding sites of SAF. SAF engages in hydrophobic interactions with certain amino acid residues,

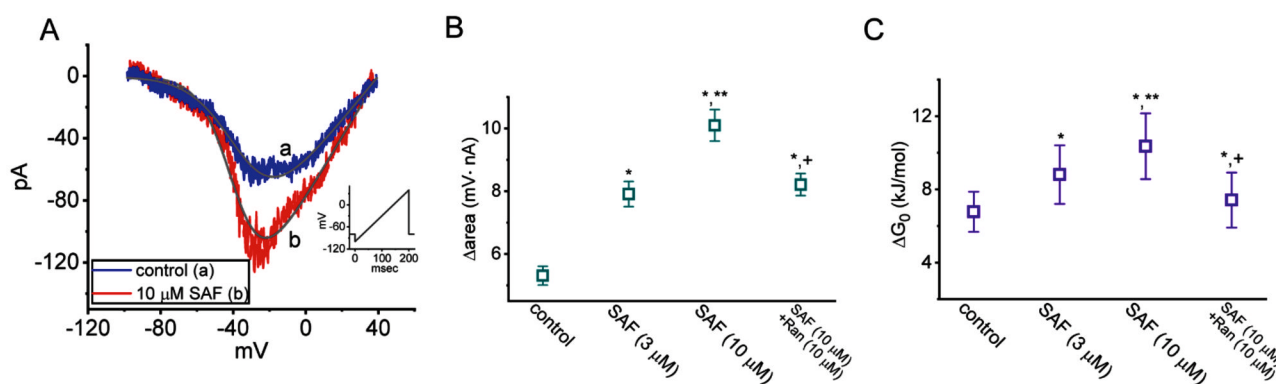


Fig. 7 Stimulatory effects of SAF on window I_{Na} [$I_{Na(W)}$] induced by an ascending ramp voltage V_{ramp} in GH₃ cells. For the experiments, the test cells were maintained at -80 mV and subjected to V_{ramp} ranging from -100 to $+40$ mV over 200 ms (ramp speed of 0.7 mV/ms). **(A)** $I_{Na(W)}$ trace in the absence (a, blue) and presence (b, red) of $10 \mu\text{M}$ SAF. The inset indicates the V_{ramp} protocol, and the downward deflection indicates inward-directed current. The continuous gray lines corresponding to the untreated or SAF-treated ($10 \mu\text{M}$) cells were fitted (least-squares minimization) with the Boltzmann equation. The values of $V_{1/1}$ and q (apparent gating charge) induced by ascending V_{ramp} over 200 ms in the absence (blue) of SAF were, respectively, -34 mV and $2.1 e$; the corresponding values in the presence (red) of $10 \mu\text{M}$ SAF were -38 mV and $2.8 e$, respectively. **(B)** Summary graph illustrating the effects of SAF (3 and $10 \mu\text{M}$) and SAF ($10 \mu\text{M}$) plus Ran ($10 \mu\text{M}$) on the Δarea of $I_{Na(W)}$ in GH₃ cells (mean \pm standard error of the mean; $n = 7$ for each point). The value of Δarea was measured at a voltage ranging from -80 and $+40$ mV, which corresponded to $I_{Na(W)}$ induced by the ascending V_{ramp} . The statistical analyses were done by ANOVA-1, $P < 0.05$, followed by post-hoc Fisher's least-significant different test, $P < 0.05$. *Significantly different from the control ($P < 0.05$), **significantly different from the SAF ($3 \mu\text{M}$) alone group ($P < 0.05$), and +significantly different from the SAF ($10 \mu\text{M}$) alone group ($P < 0.05$). **(C)** Summary graph illustrating the effects of SAF (3 and $10 \mu\text{M}$) and SAF plus Ran ($10 \mu\text{M}$) on ΔG_0 (mean \pm standard error of the mean; $n = 7$ for each point). The estimation of ΔG_0 for the induction of instantaneous $I_{Na(W)}$ is described in the Materials and Methods section. Notably, increasing the concentration of SAF increased ΔG_0 in GH₃ cells; further addition of Ran effectively reversed the SAF-induced increase in ΔG_0 . The statistical analyses were done by ANOVA-1, $P < 0.05$, followed by post-hoc Fisher's least-significant different test, $P < 0.05$. *Significantly different from the control ($P < 0.05$), **significantly different from the SAF ($3 \mu\text{M}$) alone group ($P < 0.05$), and +significantly different from the SAF ($10 \mu\text{M}$) alone group ($P < 0.05$)

such as Phe 103, Val 106, Arg 120, Asp 123, Arg 127, Thr 479, and Glu 483. In addition to interacting with intramolecular hydrogen bonds [58], SAF forms three hydrogen bonds with the Na_V -channel residues Pro 104, His 115, and Trp 119, with the bond lengths being 2.81, 3.16, and 2.90 Å, respectively. The binding affinity for the interaction between SAF and MAO-B is -7.8 kcal/mol, and the upper and lower root-mean-square deviations (RMSD) in atomic positions were 49.76 and 60.68, respectively. In line with the findings of relevant studies [21, 23, 59], we observed that the interaction between MAO-B and SAF resulted in a substantial decrease in MAO-B activity.

We further explored the molecular docking between Na_V channels and SAF. Figure 11 and Supplementary Fig. 1 depicts the predicted binding sites of SAF. After docking, SAF forms a hydrogen bond with Lys 63, with the bond length being 2.97 Å. SAF further engages in hydrophobic interactions with several residues, including Ile 9, Gln 15, Tyr 67, Asn 78, Ser 112, and Val 113. The binding affinity for the interaction between SAF and a Na_V channel was found to be -6.8 kcal/mol, and the upper and lower RMSD values were 23.00 and 25.59, respectively. The affinity energy was close to the estimated ΔG_0 for the induction of $I_{Na(W)}$ by V_{ramp} in the

presence of SAF. Thus, SAF can dock with both MAO-B and Na_V channels, thereby presumably reducing structural constraints and increasing channel activity. Collectively, the dual effects of SAF on MAO-B and Na_V channel activities [23] may considerably affect the functional activities and thus may be beneficial in the treatment of various neurological disorders [11, 15, 25, 29]. However, since a prokaryotic Na_V channel (i.e., Na_VM) was used in this prediction, whether SAF can modulate the function of Na_VM as observed in GH₃-cells' Na_V channel needs to be further examined.

Discussion

Our key findings are as follows. SAF stimulated I_{Na} in a concentration-, time-, and frequency-dependent manner. It differentially stimulated $I_{Na(T)}$ and $I_{Na(L)}$ induced by short depolarizing pulses. SAF increased the time constant of the decay of $I_{Na(T)}$ induced by a train of depolarizing pulses but increased the strength and ΔG_0 of V_{ramp} -induced $I_{Na(W)}$. The $\text{Hys}_{(V)}$ strength of $I_{Na(P)}$ (in both low- and high-threshold loops) was greater when the cells were exposed to an upright isosceles-triangular V_{ramp} . Cell-attached single-channel current recordings revealed a SAF-induced increase in the open-state probability of the channel

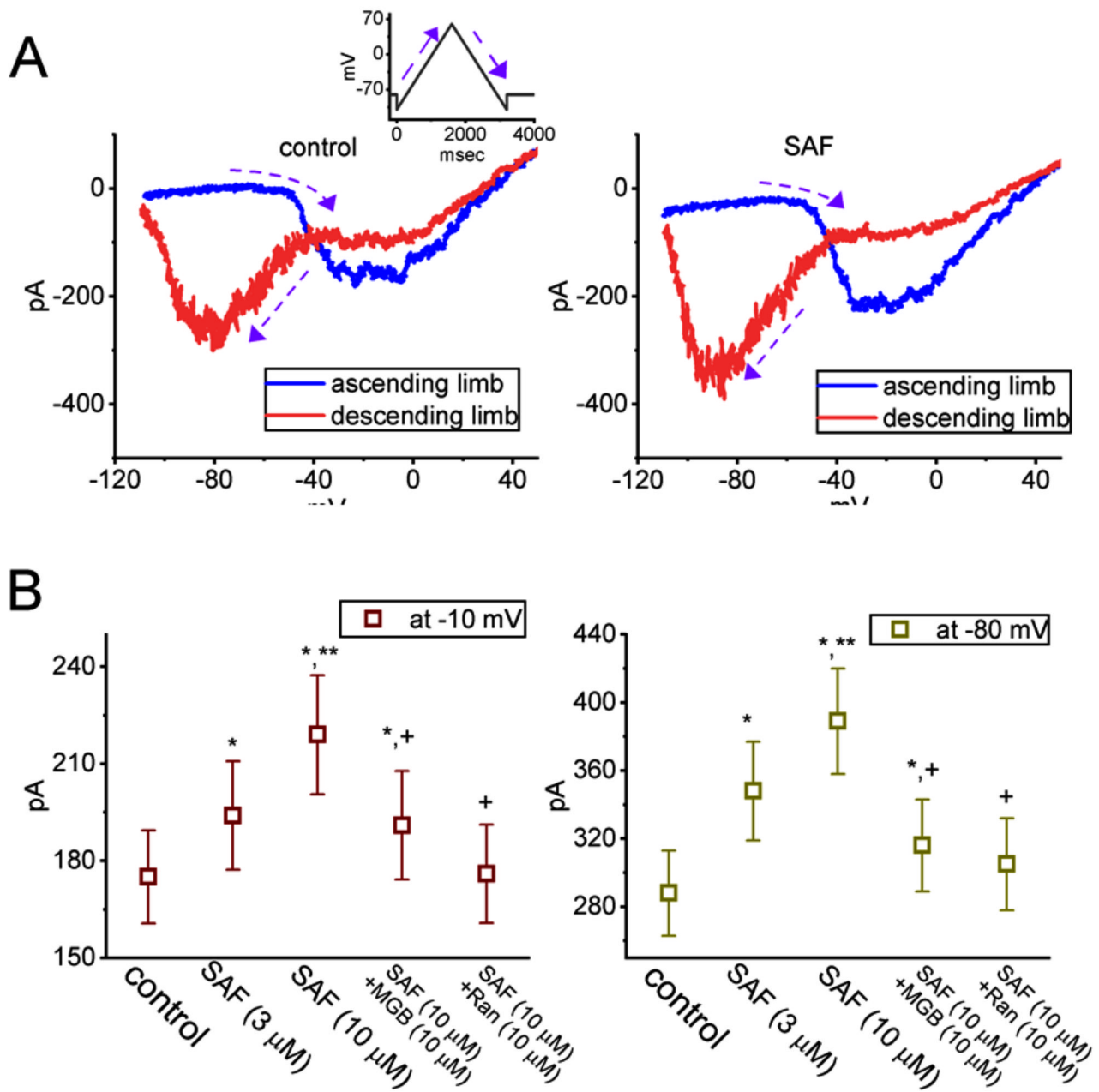


Fig. 8 Stimulatory effects of SAF on the voltage-dependent hysteresis [Hys_(V)] behavior of persistent I_{Na} [$I_{Na(P)}$] induced by upright isosceles-triangular V_{ramp} . V_{ramp} was supplied for 3.2 s (ramp speed of 0.1 mV/ms; digital-to-analog conversion) to induce Hys_(V) behavior in GH₃ cells. **(A)** Current traces during the control period (left) and during the exposure to 10 μM SAF (right). The blue and red traces shown in each panel represent currents induced by the upsloping (ascending) and downsloping (descending) limbs of the upright isosceles-triangular V_{ramp} , respectively. The inset indicates the voltage protocol. The dashed arrows indicate the direction of the current trajectory over time. **(B)** Summary graphs illustrating the effects of SAF (3 and 10 μM), SAF plus MGB, and SAF plus Ran on the amplitude of V_{ramp} -induced $I_{Na(P)}$ measured at -10 mV (ascending limb; left side) and -80 mV (descending limb; right side). Each point represents the mean ± standard error of the mean (n = 7). *Significantly different from the control (P < 0.05), **significantly different from the SAF (3 μM) alone group (P < 0.05), and +significantly different from the SAF (10 μM) alone group (P < 0.05)

without any change in the single-channel amplitude. Molecular docking between SAF and both MAO-B and Na_v channels indicated the existence of similar

structural motifs, which facilitate SAF binding to MAO-B and Na_v channels. SAF may reach the binding site once the Na_v channel protein is highly activated

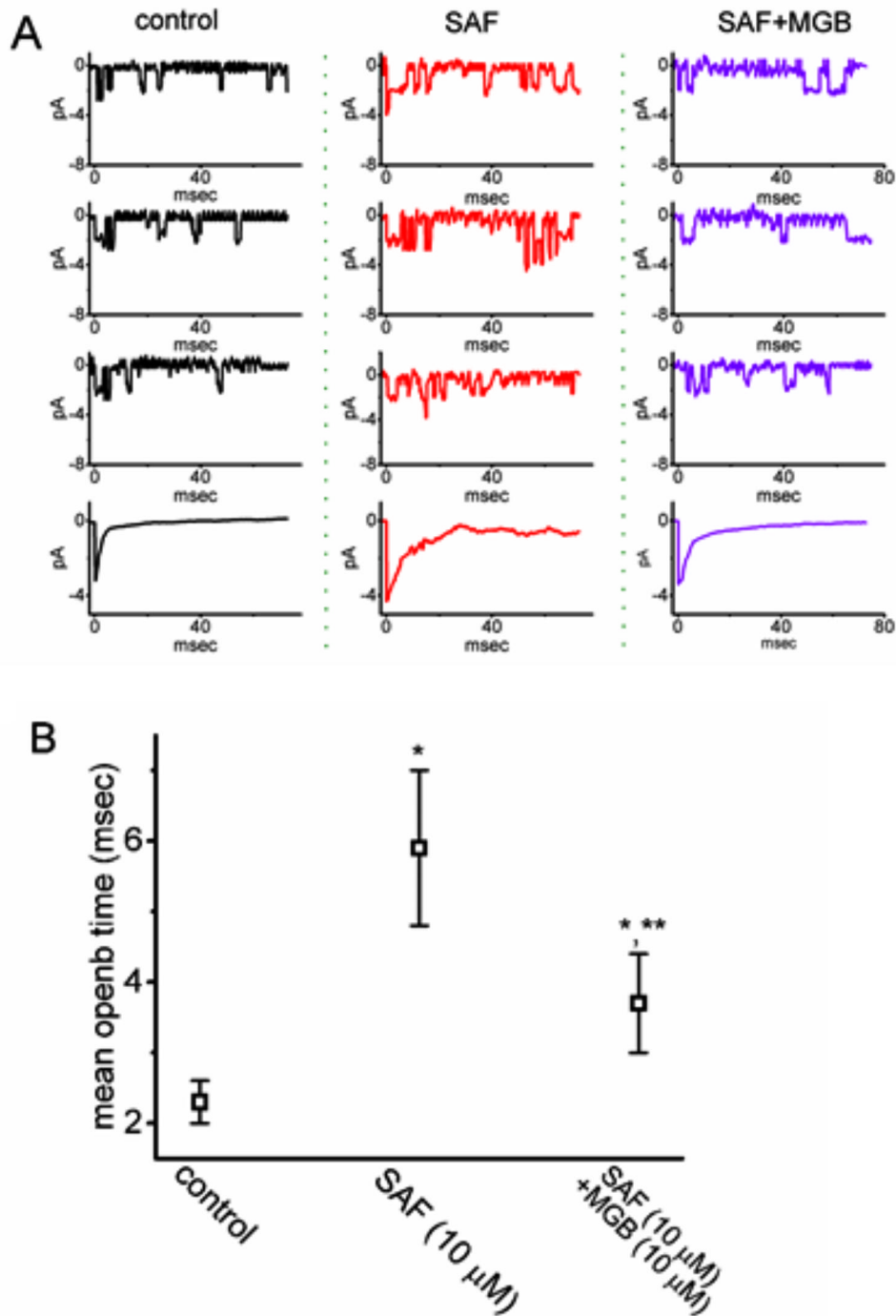


Fig. 9 Effects of SAF on single-channel Na_V currents in GH_3 cells. In **(A)**, single-channel currents were induced through successive depolarizations (rate of 0.1 Hz) from a holding potential of -100 to -10 mV. Black graphs on the left indicate current traces during the control period (in the absence of SAF or SAF plus MGB); the red and blue graphs indicate the exposure to $10 \mu M$ SAF and $10 \mu M$ SAF plus $10 \mu M$ MGB, respectively. In the SAF plus MGB experiment, MGB was added 2 min after the addition of SAF. Channel opening in each record is shown as a downward deflection; the lowest traces on each side represent the average of 50 sweeps. Notably, SAF effectively increased the open-state probability of Na_V channels, but the subsequent addition of MGB attenuated the SAF-induced increase in the likelihood of channel opening. However, the presence of neither SAF nor MGB in addition to SAF changed the single-channel amplitude of Na_V channels in GH_3 cells. **(B)** Graph showing effects of SAF, SAF plus MGB on the mean open time of Na_V channel (mean \pm standard error of the mean; $n = 7$). *Significantly different from control ($P < 0.05$) and **significantly different from SAF ($10 \mu M$) alone group ($P < 0.05$)

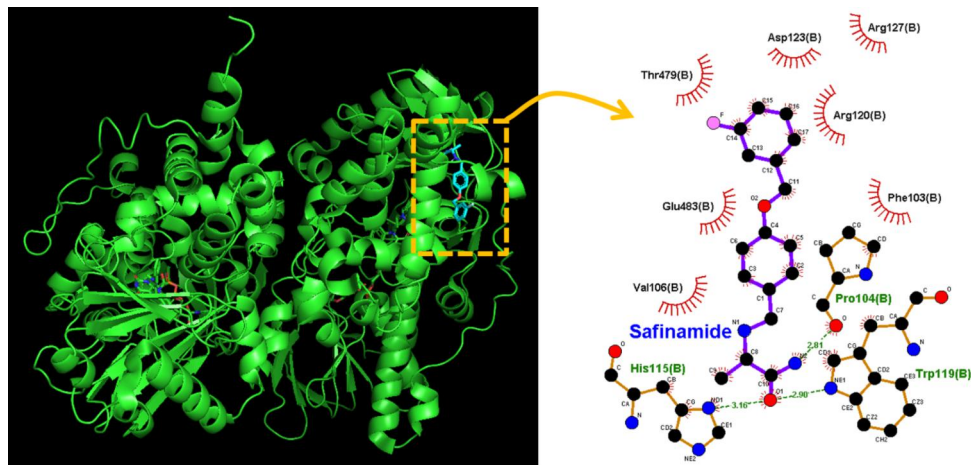


Fig. 10 Predicted docking interactions between SAF and monoamine oxidase B (MAO-B). The protein structure was obtained from the Protein Data Bank (ID: 1GOS); the chemical structure of SAF was obtained from PubChem [compound CID: 131682 (3D conformer)]. MAO-B was docked with SAF (yellow dashed box on the left) through PyRx, and the corresponding interaction diagram was generated using LigPlot⁺. The red arcs with spokes radiating toward the ligand (SAF) indicate hydrophobic interactions between SAF and MAO-B. The green dotted line indicates the hydrogen bond between SAF and Pro 104, His 115, or Trp 119, with the corresponding bond lengths being 2.81, 3.16, or 2.90 Å

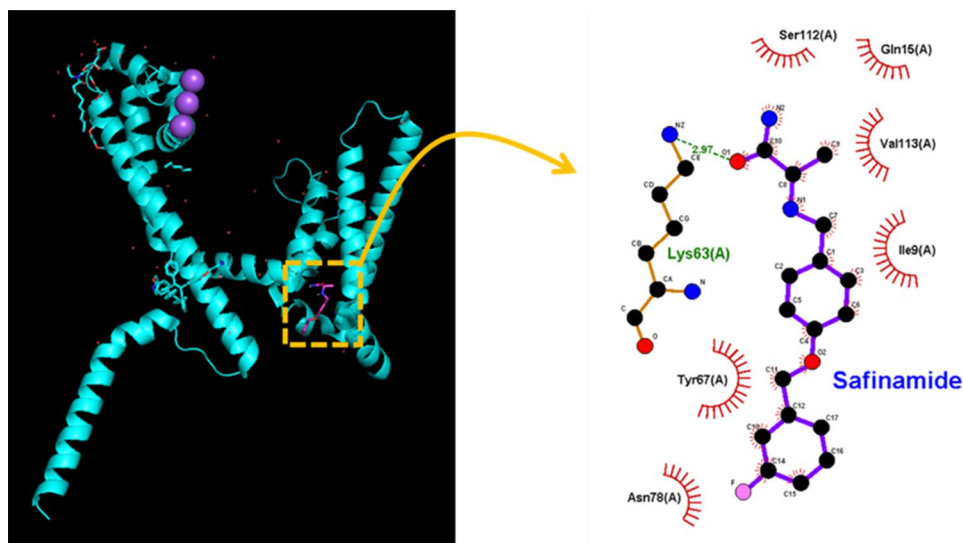


Fig. 11 Predicted docking interactions between Na_v channels and SAF. The protein structure of a Na_v channel was obtained from the Protein Data Bank (ID: 6Z8C), and the chemical structure of SAF was obtained from PubChem [compound CID: 131682 (3D conformer)]. A Na_v channel was docked with SAF (yellow dashed box on the left) using PyRx; the corresponding interaction diagram was generated using LigPlot⁺. In the image on the right, the red arcs with spokes radiating toward the ligand (SAF) indicate hydrophobic interactions between SAF and several amino acid residues, whereas the green dashed line indicates the hydrogen bond between SAF and Lys 63, the length of which was 2.97 Å. The docking regions appear to be adjacent to the transmembrane region (position: residues 82–102) and the membrane segment (position: residues 46–67). The interactions probably alter structural constraints, thereby increasing the open-state probability of Na_v channels

and is in its open state or conformation. Overall, these findings suggest that SAF-mediated modulation of the magnitude, gating, and Hys_(V) behavior of I_{Na} may be independent and upstream of its inhibitory action on MAO-B activity.

As mentioned, SAF inhibits the activity of MAO-B [2, 14, 23, 24, 52, 53, 60]. Thus, in the present study, the stimulation of I_{Na} by SAF was expected to be associated

with the inhibition of MAO-B by SAF and with subsequent increases in the concentrations of dopamine and serotonin. However, the exposure of cells to dopamine and serotonin did not lead to any changes in the magnitude of $I_{Na(T)}$ induced by rapid membrane depolarization pulses. Adding dopamine and serotonin separately to the bath solution in the presence of SAF exerted no effects on the SAF-stimulated $I_{Na(T)}$. Therefore, the stimulatory

effects of SAF on $I_{\text{Na(T)}}$ and $I_{\text{Na(L)}}$ may be mediated by a mechanism other than that involving the inhibition of MAO-B activity.

The time-dependent decrease in $I_{\text{Na(T)}}$ induced by a 20-Hz train of depolarizing pulses (40-ms pulses of voltage ascending from -80 to -10 mV; rate of 20 Hz; duration of 1 s) was decelerated by SAF. The results indicate that there is use dependence of $I_{\text{Na(T)}}$ during repetitive depolarization, as demonstrated previously [34–36, 60]. SAF may lead to progressive gain-of-function changes by altering and decelerating the inactivation of currents. Thus, the SAF-mediated increase in $I_{\text{Na(T)}}$ may be closely associated with use-dependent attenuation of the magnitude of $I_{\text{Na(T)}}$ induced by a train of depolarizing pulse stimuli.

We further estimated the Δarea and ΔG_0 values for the instantaneous $I_{\text{Na(W)}}$ induced by an ascending V_{ramp} , both of which were found to be markedly higher when SAF was present. Adding Ran in the presence of SAF reversed the SAF-mediated increase in the Δarea and ΔG_0 of the current. Because the magnitude of $I_{\text{Na(W)}}$ is primarily responsible for the background (steady state) conductance of Na^+ and the electrical firing of excitable cells [37, 38, 41, 61–63], SAF may increase the firing frequency of action potentials by enhancing the strength of $I_{\text{Na(W)}}$. It is important to note that the currents elicited by V_{ramp} may also result from late/persistent I_{Na} and slow closed-state inactivation. Whether the SAF-mediated augmentation of ramp currents was caused by increasing $I_{\text{Na(W)}}$ still needs to be investigated. Moreover, how the activation energy of V_{ramp} -induced $I_{\text{Na(W)}}$ can be increased in the SAF presence remains to be further studied.

We observed the nonlinear voltage-dependent $\text{Hys}_{(\text{V})}$ behavior of $I_{\text{Na(P)}}$ during the control period and the exposure of the cells to SAF, SAF plus MGB, or SAF plus Ran [36, 42]. The $\text{Hys}_{(\text{S})}$ behavior was induced by exposing the cells to an upright isosceles-triangular V_{ramp} for 3.2 s. SAF increased the peak of $I_{\text{Na(P)}}$ induced by the ascending (upsloping) limb of the triangular V_{ramp} , particularly at -10 mV, and the amplitude of $I_{\text{Na(P)}}$ induced by the descending (downsloping) end of V_{ramp} , particularly at -80 mV. Thus, we noted a figure-of-eight (∞ -shaped) configuration of the $\text{Hys}_{(\text{V})}$ loop of current induced by the triangular V_{ramp} ; the strength of this behavior was discovered to be considerably enhanced in the presence of SAF. Thus, V_{ramp} induced two distinct types of $I_{\text{Na(P)}}$: high-threshold current and low-threshold current. The high-threshold $I_{\text{Na(P)}}$ was excessively induced [at a voltage range where peak $I_{\text{Na(T)}}$ was induced maximally] by the upsloping limb of the triangular V_{ramp} ; by contrast, the low-threshold $I_{\text{Na(P)}}$ was induced by the downsloping end of the triangular V_{ramp} . Furthermore, the trajectories of currents induced by

the ascending and descending limbs of the triangular V_{ramp} followed the counterclockwise and clockwise directions, respectively. Adding MGB and Ran separately in the presence of SAF reduced the SAF-mediated increases in high- and low-threshold $I_{\text{Na(P)}}$ induced by V_{ramp} . It also needs to be noted that the increase of the current at -80 mV in the descending limb of the voltage protocol might be caused by the ability of SAF to activate the persistent I_{Na} . Thus, whether SAF affect the Na_V -channel deactivation still warrants further investigations.

It needs to be noted that as the concentration of extracellular Ca^{2+} was decreased, the gating of I_{Na} might be altered [64]. However, the presence of extracellular Ca^{2+} was also allowed to activate voltage-gated Ca^{2+} current and then to interfere with the examination of voltage-gated Na^+ current. Therefore, whether safinamide affects the amplitude and gating of I_{Na} when the concentration of external Ca^{2+} is within the physiological range remains to be further studied.

The cell-attached current recordings revealed that SAF increased the open-state probability of Na_V ; this increase was reversed by the subsequent addition of MGB. Furthermore, SAF extended the mean open time of single Na_V channels; however, this effect of SAF was reversed by MGB. SAF did not modify the amplitude of single Na_V channels; this indicates that the interaction between SAF and Na_V channels is secondary to alterations, which possibly occur at a location remote from the pore region of the channels.

Pharmacokinetic studies have reported that the maximal plasma concentrations of SAF after single 2.5, 5.0, and 10.0 mg/kg doses can be approximately 1000, 2500, and 5500 ng/mL (or 3.3, 8.3 and 18.2 μM), respectively [65]. The EC_{50} values for the SAF-mediated stimulation of $I_{\text{Na(T)}}$ and $I_{\text{Na(L)}}$ were 27.1 ± 2.1 and 4.8 ± 0.7 μM , respectively; this indicates that the stimulatory effects of SAF on I_{Na} are within the clinical therapeutic range, although the SAF concentration in cerebrospinal fluid is still unclear [60]. The IC_{50} for the SAF-mediated inhibition of MAO-B activity has been reported to be approximately 30–40 nM [23]. Notably, the magnitude of SAF-stimulated I_{Na} depends strongly on various factors, including the pre-existing resting potential, the firing pattern of the action potential, the concentration of SAF in cells, and a combination of the aforementioned factors. Regarding the inhibitory effect of SAF on MAO-B, SAF may lyse and remove the components of the surface membrane of various host cells (Edmondson and Binda, 2018), thus accessing cytosolic or mitochondrial enzymes. Thus, the stimulatory perturbation of I_{Na} [$I_{\text{Na(T)}}$, $I_{\text{Na(L)}}$, $I_{\text{Na(W)}}$, and $I_{\text{Na(P)}}$] is clinically achievable by using SAF and may have pharmacological, therapeutic, and toxicological relevance in humans [12, 16, 17].

SAF may increase blood pressure. Na_V channels are functionally distributed across vascular smooth muscle cells [66–68]. The mRNA transcripts of the α subunits of $\text{Na}_V1.1$, $\text{Na}_V1.2$, $\text{Na}_V1.3$, and $\text{Na}_V1.6$, together with those of the $\beta 1$ and $\beta 3$ subunits, have been detected in GH_3 cells [69]. The extent to which SAF-induced hypertensive events [4, 10] are associated with the stimulatory effects of SAF on I_{Na} in vascular smooth muscle cells (i.e., $\text{Na}_V1.7$), heart cells (i.e., $\text{Na}_V1.5$ or $\text{Na}_V1.6$), and skeletal muscle cells (i.e., $\text{Na}_V1.4$) is worth investigation.

In contrast to our findings, earlier studies showed SAF might suppress I_{Na} magnitude in different preparations [21, 26–29]. It will be important to determine whether the inhibitory effect of SAF on I_{Na} is associated with either the decrease of the activity of monoamine oxidase or the production of reactive oxygen species [13, 14, 22–25]. Of note, although SAF was considered a potential anticonvulsant based on prior reports of I_{Na} attenuating property, clinically, the anticonvulsive activity of SAF was not proven, as only open-label studies comparing with baseline were provided [70, 71]. The inhibitor of Na_V channels could generally be considered as an anticonvulsant, however, despite the unclear underlying ionic mechanism, the stimulator of Na_V channels virtually might not become a pro-epileptic drug, because of a wide range of epileptic disorders through which the initiation or epileptogenesis is largely unclear. Furthermore, the difference on the effect of I_{Na} may be the result of dissimilar channel isoforms, expression levels of isoforms, the species, the auxiliary proteins in the cell types, and the different concentrations of compounds used for each cell type. Direct comparisons of sodium channel kinetic properties were thus restricted to data within the same cell type. Nevertheless, it is likely that the stimulatory effect of SAF on I_{Na} is preferentially linked to its bindings to $\text{Na}_V1.5$ and/or $\text{Na}_V1.6$ isoforms of the channel. Further characterization and interpretation of the modulatory effect of SAF on I_{Na} and overall cellular excitability in different cell types or network should be implemented.

Supplementary Information

The online version contains supplementary material available at <https://doi.org/10.1186/s40360-024-00739-5>.

Supplementary Material 1

Author contributions

TYH, SNW, and CWH conceived the study. TYH, SNW, and CWH performed the experiments. SNW and CWH participated in the statistical analysis. All authors approved the final manuscript. Each author contributed substantially during manuscript drafting or revision.

Funding

This work was supported in part by grants from the National Science and Technology Council (111-2314-B-006 -103 -MY2), Taiwan and the National Cheng Kung University Hospital (NCKUH-11201005) Tainan, Taiwan.

Data availability

The datasets used and/or analyzed during the current study are available from the corresponding author on reasonable request.

Declarations

Ethics approval and consent to participate

Not applicable. This study did not involve human participants and animals.

Consent for publication

Not applicable.

Conflicts of interest

The authors declare no conflicts of interest. The funders had no role in the design of the study; in the collection, analyses, or interpretation of data, in the writing of the manuscript, or in the decision to publish the results.

Received: 9 September 2023 / Accepted: 30 January 2024

Published online: 08 February 2024

References

- Maj R, Fariello R, Pevarello P, Varasi M, McArthur RA, Salvati P. Anticonvulsant activity of PNU-151774E in the amygdala kindled model of complex partial seizures. *Epilepsia*. 1999;40:1523–28.
- Caccia C, Maj R, Calabresi M, Maestroni S, Faravelli L, Curatolo L, Salvati P, Fariello RG. Safinamide: from molecular targets to a new anti-Parkinson drug. *Neurology*. 2006;67:S18–S23.
- Müller T. Current status of safinamide for the drug portfolio of Parkinson's disease therapy. *Expert Rev Neurother*. 2013;13:969–77.
- Marquet A, Kupas K, Johnne A, Astruc B, Patat A, Krösser S, Kovar A. The effect of safinamide, a novel drug for Parkinson's disease, on pressor response to oral tyramine: a randomized, double-blind, clinical trial. *Clin Pharmacol Ther*. 2012;92:450–57.
- Dézsi L, Vécsei L. Safinamide for the treatment of Parkinson's disease. *Expert Opin Investig Drugs*. 2014;23:729–42.
- Teixeira FG, Gago MF, Marques P, Moreira PS, Magalhães R, Sousa N, Salgado AJ. Safinamide: a new hope for Parkinson's disease? *Drug Discov Today*. 2018;23:736–44. <https://doi.org/10.1016/j.drudis.2018.01.038>.
- Tsuboi Y, Hattori N, Yamamoto A, Sasagawa Y, Nomoto M, ME2125-4 Study Group. Long-term safety and efficacy of safinamide as add-on therapy in levodopa-treated Japanese patients with Parkinson's disease with wearing-off: results of an open-label study. *J Neurol Sci*. 2020;416:117012. <https://doi.org/10.1016/j.jns.2020.117012>.
- Tsuboi Y, Koebis M, Kogo Y, Ishida T, Suzuki I, Nomoto M, Hattori N. Effects of safinamide adjunct therapy on pain in patients with Parkinson's disease: post-hoc analysis of a Japanese phase 2/3 study. *J Neurol Sci*. 2021;429:118070. <https://doi.org/10.1016/j.jns.2021.118070>.
- Stocchi F, Antonini A, Berg D, Bergmans B, Jost W, Katzenschlager R, Kulisevsky J, Odin P, Valldeoriola F, Ray Chaudhuri K. Safinamide in the treatment pathway of Parkinson's disease: a European Delphi consensus. *NPJ Parkinsons Dis*. 2022;8:17.
- Stocchi F, Vacca L, Grassini P, Tomino C, Caminiti G, Casali M, D'Antoni V, Volterrani M, Torti M. Overnight switch from rasagiline to safinamide in Parkinson's disease patients with motor fluctuations: a tolerability and safety study. *Eur J Neurosci*. 2021;28:349–54. <https://doi.org/10.1111/ejn.15072>.
- Wasan H, Singh D, Kh R. Safinamide in neurological disorders and beyond: evidence from preclinical and clinical studies. *Brain Res Bull*. 2021;168:165–77. <https://doi.org/10.1016/j.brainresbull.2020.12.020>.
- Abbruzzese G, Kulisevsky J, Bergmans B, Gomez-Esteban JC, Kagi G, Raw J, Stefani A, Warnecke T, Jost WH, SYNAPSES Study Investigators Group. A European observational study to evaluate the safety and the effectiveness of safinamide in routine clinical practice: the SYNAPSPSE trial. *J Parkinson's Dis*. 2022;12:473.
- Hattori N, Kogo Y, Koebis M, Ishida T, Suzuki I, Tsuboi Y, Nomoto M. The effects of safinamide adjunct therapy on depression and apathy in patients with Parkinson's disease: post-hoc analysis of a Japanese phase

- 2/3 study. *Front Neurol.* 2022;12:752632. <https://doi.org/10.3389/fneur.2021.752632>.
14. Jost WH. A critical appraisal of MAO-B inhibitors in the treatment of Parkinson's disease. *J Neural Transm (Vienna).* 2022;129:723–36.
 15. Kurihara K, Mishima T, Fujioka S, Tsuboi Y. Efficacy and safety evaluation of safinamide as an add-on treatment to levodopa for Parkinson's disease. *Expert Opin Drug Saf.* 2022;21:137–47.
 16. Nomoto M, Ishida T, Koebis M, Kamei T, Suzuki I, Hattori N, Tsuboi Y. Characteristics of wearing-off and motor symptoms improved by safinamide adjunct therapy in patients with Parkinson's disease: a post-hoc analysis of a Japanese phase 2/3 study. *J Neuro Sci.* 2022;434:120083.
 17. Rodríguez-Jorge F, Beltrán-Corbellini Á, Chico-García JL, Parra-Díaz P, Baena-Álvarez B, Pagonabarraga J, Pérez-Torre P, Pareés I, López-Sendón JL, Martínez-Castrillo JC. Efficacy and safety of high doses of safinamide in advanced Parkinson disease. *Parkinsonism Relat Disord.* 2022;97:73–74.
 18. Santos García D, Cabo López I, Labandeira Guerra C, Yáñez Baña R, Cimas Hernando MI, Paz González JM, Alonso Losada MG, Gonzalez Palmás MJ, Cores Bartolomé C, Martínez Miró C. Safinamide improves sleep and daytime sleepiness in Parkinson's disease: results from the SAFINONMOTOR study. *Neurol Sci.* 2022;43:2537–44.
 19. Antonini A, Moro E, Godeiro C, Reichmann H. Medical and surgical management of advanced Parkinson's disease. *Mov Disord.* 2018;33:900–08.
 20. Rizzone MG, Mancini F, Artusi CA, Balestrino R, Bonvegna S, Fabbri M, Imbalzano G, Montanaro E, Romagnolo A, Zibetti M. Efficacy of safinamide as add-on therapy after subthalamic nucleus deep brain stimulation in Parkinson disease. *Neurol Sci.* 2022;43:3187–93.
 21. Binda C, Milczek EM, Bonivento D, Wang J, Mattevi A, Edmondson DE. Lights and shadows on monoamine oxidase inhibition in neuroprotective pharmacological therapies. *Curr Top Med Chem.* 2011;11:2788–96.
 22. Edmondson DE, Binda C. Monoamine oxidases. *Subcell Biochem.* 2018;87:117–39.
 23. Elkamhawy A, Paik S, Park JH, Kin HJ, Hassan AHE, Lee K, Park KD, Roh EJ. Discovery of novel and potent safinamide-based derivatives as highly selective hMAO-B inhibitors for treatment of Parkinson's disease (PD): design, synthesis, in vitro, in vivo, and in silico biological studies. *Bioorg Chem.* 2021;115:105233. <https://doi.org/10.1016/j.bioorg.2021.105233>.
 24. Tan YY, Jenner P, Chen SD. Monoamine oxidase-B inhibitors for the treatment of Parkinson's disease: past, present, and future. *J Parkinsons Dis.* 2022;12:477–93. <https://doi.org/10.3233/JPD-219001>.
 25. Gu X, Zhang G, Qin Z, Yin M, Chen W, Zhang Y, Liu X. Safinamide protects against amyloid β (β)-induced oxidative stress and cellular senescence in M17 neuronal cells. *Bioengineered.* 2022;13:1921–30. <https://doi.org/10.1080/21655979.2022.2036827>.
 26. Fariello RG, McArthur RA, Bonsignori A, Cervini MA, Maj R, Marrari P, Pevarello P, Wolf HH, Woodhead JW, White HS. Preclinical evaluation of PNU-151774E as a novel anticonvulsant. *J Pharmacol Exp Ther.* 1998;285:397–403. [https://doi.org/10.1016/s0022-3956\(98\)00100-8](https://doi.org/10.1016/s0022-3956(98)00100-8).
 27. Pevarello P, Bonsignori A, Caccia C, Amici R, Salvati P, Fariello RG, McArthur RA, Varasi M. Sodium channel activity and sigma binding of 2-amino-propanamide anticonvulsants. *Bioorg Med Chem Lett.* 1999;9:2521–24.
 28. Salvati P, Maj R, Caccia C, Cervini MA, Fornaretto MG, Lamberti E, Pevarello P, Skeen GA, White HS, Wolf HH. Biochemical and electrophysiological studies on the mechanism of action of PNU-151774E, a novel antiepileptic compound. *J Pharmacol Exp Ther.* 1999;288:1151–59.
 29. Desaphy JF, Farinato A, Altamura C, De Bellis M, Imbrici P, Tarantino N, Caccia C, Melloni E, Padoani G, Vailati S. Safinamide's potential in treating nondystrophic myotonias: inhibition of skeletal muscle voltage-gated sodium channels and skeletal muscle hyperexcitability in vitro and in vivo. *Exp Neurol.* 2020;328:113287.
 30. Catterall WA, Goldin AL, Waxman SG. International union of pharmacology: XLVII. Nomenclature and structure-function relationships of voltage-gated sodium channels. *Pharmacol Rev.* 2005;57:397–409.
 31. Wang YJ, Lin MW, Lin AA, Wu SN. Riluzole-induced block of voltage-gated Na^+ current activation of BKCa channels in cultured differentiated human skeletal muscle cells. *Life Sci.* 2008;82:11–20. <https://doi.org/10.1016/j.lfs.2007.10.029>.
 32. Stojilkovic SS, Tabak J, Bertram R. Ion channels and signaling in the pituitary gland. *Endocr Rev.* 2010;31:845–915. <https://doi.org/10.1210/er.2009-0033>.
 33. Huang CW, Hung TY, Wu SN. The inhibitory actions by lacosamide, a functionalized amino acid, on voltage-gated Na^+ currents. *Neuroscience.* 2015;287:125–36.
 34. Navarro MA, Salari A, Lin JL, Cowan LM, Milesco M, Milesco LS. Sodium channels implement a molecular leaky integrator that detects action potentials and regulates neuronal firing. *Elife.* 2020;9:e54940.
 35. Cho HY, Chen PC, Chuang TH, Yu MC, Wu SN. Activation of voltage-gated Na^+ current by GV-58, a known activator of CaV channels. *Biomedicines.* 2022;10:721.
 36. Wu CL, Chuang CW, Cho HY, Chuang TH, Wu SN. The evidence for effective inhibition of INa produced by mirogabalin ((1R,5S,6S)-6-(aminomethyl)-3-ethyl-bicyclo[3.2.0]hept-3-ene-6-acetic acid), a known blocker of CaV channels. *Int J Mol Sci.* 2022;23:3845. <https://doi.org/10.3390/ijms23073845>.
 37. Simasko SMA background sodium conductance is necessary for spontaneous depolarizations in rat pituitary cell line GH3. *Am J Physiol.* 1994;266(3 Pt 2):C709–19.
 38. Wang JA, Lin W, Morris T, Banderli U, Juranka PF, Morris CE. Membrane trauma and Na^+ leak from Nav1.6 channels. *Am J Physiol Cell Physiol.* 2009;297:C823–34. <https://doi.org/10.1152/ajpcell.00553.2008>.
 39. Wu SN, Wu YH, Chen BS, Lo YC, Liu YC. Underlying mechanism of actions of tefluthrin, a pyrethroid insecticide, on voltage-gated ion currents and on action currents in pituitary tumor (GH3) cells and GnRH-secreting (GT1-7) neurons. *Toxicology.* 2009;258:70–77. <https://doi.org/10.1016/j.tox.2009.01.012>.
 40. Morris CE, Boucher A, Joós B. Left-shifted Nav channels in injured bilayer: primary targets for neuroprotective Nav antagonists? *Front Pharmacol.* 2012;3:19.
 41. Yu N, Morris CE, Joós B, Longin A. Spontaneous excitation patterns computed for axons with injury-like impairments of sodium channels and Na/K pumps. *PLoS Comput Biol.* 2012;8:e1002664.
 42. Chang WT, Wu SN. Characterization of direct perturbations on voltage-gated sodium current by esaxerenone, a nonsteroidal mineralocorticoid receptor blocker. *Biomedicines.* 2021;9:549.
 43. Chang WT, Wu SN. Effectiveness of columbianadin, a bioactive coumarin derivative, in perturbing transient and persistent INa. *Int J Mol Sci.* 2021;22:621.
 44. Chang WT, Liu PY, Gao ZH, Lee SW, Lee WK, Wu SN. Evidence for the effectiveness of remdesivir (GS-5734), a nucleoside-analog antiviral drug in the inhibition of I_{K(M)} or I_{K(DR)} and in the stimulation of I_{MEP}. *Front Pharmacol.* 2020;11:1091.
 45. Yifrach O, MacKinnon R. Energetics of pore opening in a voltage-gated K⁺ channel. *Cell.* 2002;111:231–39. [https://doi.org/10.1016/S0092-8674\(02\)01011-7](https://doi.org/10.1016/S0092-8674(02)01011-7).
 46. Hsiao HT, Lu GL, Liu YC, Wu SN. Effective perturbations of the amplitude, gating, and hysteresis of IK(DR) caused by PT-2385, an HIF-2 α inhibitor. *Membranes.* 2021;11:636.
 47. Chen BS, Lo YC, Peng H, Hsu TI, Wu SN. Effects of ranolazine, a novel anti-anginal drug, on ion currents and membrane potential in pituitary tumor GH3 cells and NG108-15 neuronal cells. *J Pharmacol Sci.* 2009;110:295–305.
 48. Chuang TH, Cho HY, Wu SN. The evidence for sparsentan-mediated inhibition of INa and IK(erg), possibly unlinked to its antagonism of angiotensin II or endothelin type a receptor. *Biomedicines.* 2021;10:86.
 49. Wu SN, Huang CW. Editorial to the special issue "electrophysiology". *Int J Mol Sci.* 2021;22:2956. <https://doi.org/10.3390/ijms22062956>.
 50. Liu J, Tu H, Zhang D, Zheng H, Li YL. Voltage-gated sodium channel expression and action potential generation in differentiated NG108-15 cells. *BMC Neurosci.* 2012;13:129.
 51. Zhang J, Yuan H, Yao X, Chen S. Endogenous ion channels expressed in human embryonic kidney (HEK-293) cells. *Pflügers Arch.* 2022;474:665–80.
 52. Abeles RH, Tashjian Jr AH. Inhibition of monoamine oxidase activity by propargylamine in pituitary cells in culture: lack of effect on cell growth or prolactin production. *Biochem Pharmacol.* 1974;23:2205–07.
 53. Kier A, Han J, Jacobson L. Chronic treatment with the monoamine oxidase inhibitor phenelzine increases hypothalamic-pituitary-adrenocortical activity in male C57BL/6 mice: relevance to atypical depression. *Endocrinology.* 2005;146:1338–47.
 54. Cossette P, Loukas A, Lafrenière RG, Rochefort D, Harvey-Girard E, Ragsdale DS, Dunn RJ, Rouleau GA. Functional characterization of the

- D188V mutation in neuronal voltage-gated sodium channel causing generalized epilepsy with febrile seizures plus (GEFS). *Epilepsy Res.* 2003;53:107–17.
55. Wu SN, So EC, Liao YK, Huang YM. Reversal by ranolazine of doxorubicin-induced prolongation in the inactivation of late sodium current in rat dorsal root ganglion neurons. *Pain Med.* 2015;16:1032–34. <https://doi.org/10.1111/pme.12714>.
56. Bengel P, Ahmad S, Sossalla S. Inhibition of late sodium current as an innovative antiarrhythmic strategy. *Curr Heart Fail Rep.* 2017;14:179–86.
57. So EC, Wu SN, Lo YC, Su K. Differential regulation of tefluthrin and telmisartan on the gating charges of INa activation and inactivation as well as on resurgent and persistent INa in a pituitary cell line (GH3). *Toxicol Lett.* 2018;285:104–12.
58. Pawlak T, Paluch P, Dolot R, Bujacz G, Potrzebowski MJ. New salts of trifluoromethyl (TFM) - single crystal X-ray and solid state NMR investigation. *Solid State Nucl Magn Reson.* 2022;122:101820.
59. Zindo FT, Malan SF, Omoruyi SI, Enogieru AB, Ekpo OE, Joubert J. Design, synthesis and evaluation of pentacycloundecane and hexacycloundecane propargylamine derivatives as multifunctional neuroprotective agents. *Eur J Med Chem.* 2019;163:83–94.
60. Müller T, Foley P. Clinical pharmacokinetics and pharmacodynamics of safinamide. *Clin Pharmacokinet.* 2017;56:251–61.
61. Nesin V, Bowman AM, Xiao S, Pakhomov AG. Cell permeabilization and inhibition of voltage-gated Ca²⁺ and Na⁺ channel currents by nanosecond pulsed electrical field. *Bioelectromagnetics.* 2012;33:394–404.
62. Frenz CT, Hansen A, Dupuis ND, Shultz N, Levinson SR, Finger TE, Dionne VE. NaV1.5 sodium channel window currents contribute to spontaneous firing in olfactory sensory neurons. *J Neurophysiol.* 2014;112:1091–104. <https://doi.org/10.1152/jn.00701.2013>.
63. Menezes LFS, Sabiá Júnior EF, Tibery DV, Carneiro LDA, Schwartz EF. Epilepsy-related voltage-gated sodium channelopathies: a review. *Front Pharmacol.* 2020;11:1276.
64. Martisuzs BJ, Tsintsadze T, Chang W, Smith SM. Enhanced excitability of cortical neurons in low-divalent solution ns is primarily mediated by altered voltage-dependence of voltage-gated sodium channels. *Elife.* 2021;10:e67914.
65. Marzo A, Dal Bo L, Monti NC, Crivelli F, Ismaili S, Caccia C, Cattaneo C, Fariello RG. Pharmacokinetics and pharmacodynamics of safinamide, a neuroprotectant with antiparkinsonian and anticonvulsant activity. *Pharmacol Res.* 2004;50:77–85.
66. Saleh S, Yeung SYM, Prestwich S, Pucovsky V, Greenwood I. Electrophysiological and molecular identification of voltage-gated sodium channels in murine vascular myocytes. *J Physiol.* 2005;568:155–69.
67. Barajas-Martinez H, Goodrow RJ, Hu D, Patel P, Desai M, Panama BK, Treat JA, Aistrup GL, Cordeiro JM. Biophysical and molecular comparison of sodium current in cells isolated from canine atria and pulmonary vein. *Pflugers Arch.* 2017;469:703–12.
68. Meguro K, Iida H, Takano H, Morita T, Sata M, Nagai R, Nakajima T. Function and role of voltage-gated sodium channel NaV1.7 expressed in aortic smooth muscle cells. *Am J Physiol Heart Circ Physiol.* 2009;296:H211–9.
69. Vega AV, Espinoza JL, Lopez-Dominguez AM, Lopez-Santiago LF, Navarrete A, Cota G. L-type calcium channel activation up-regulates the mRNAs for two different sodium channel alpha subunits (Nav1.2 and Nav1.3) in rat pituitary GH3 cells. *Brain Res Mol Brain Res.* 2003;116:115–25.
70. Committee for Medicinal Products for Human Use. Xadago: international Non-Proprietary Name: safinamide. Assessment Report. European Medicines Agency. 2014;393951.
71. Fariello RG. Safinamide. *Neurotherapeutics.* 2007;4:110–16. <https://doi.org/10.1016/j.nurt.2006.11.004>.

Publisher's Note

Springer Nature remains neutral with regard to jurisdictional claims in published maps and institutional affiliations.